Biosensors and Bioelectronics 179 (2021) 113082

Contents lists available at ScienceDirect

Biosensors and Bioelectronics

journal homepage: http://www.elsevier.com/locate/bios

A 3D electrochemical biosensor based on Super-Aligned Carbon NanoTube array for point-of-care uric acid monitoring

Muqun Yang [a,b], Han Wang [b,*], Peng Liu [c], Jing Cheng [a,b,**]

[a] Precision Medicine and Healthcare Research Center, Tsinghua-Berkeley Shenzhen Institute(TBSI), Tsinghua University, Shenzhen, 518055, China
[b] Department of Biomedical Engineering, School of Medicine, Tsinghua University, Beijing, 100084, China
[c] Tsinghua-Foxconn Nanotechnology Research Center & State Key Laboratory of Low-Dimensional Quantum Physics, Department of Physics, Tsinghua University, Beijing, 100084, China

ARTICLE INFO

Keywords:
Point-of-Care
Electrochemical biosensor
Metabolic diseases
3D electrodes
Super-aligned carbon NanoTube

ABSTRACT

Uric acid analysis is extremely important for gout prognosis, diagnosis and treatment. Previous technologies either lack specificity or exhibit poor performance, and thus could not meet the need of Point-of-Care (POC) uric acid monitoring. Here we present for the first time, a novel electrochemical biosensor based on 3D Super-Aligned Carbon NanoTube (SACNT) array to facilitate POC uric acid monitoring. The working electrode of the biosensor is composed of an orderly 3D SACNT array immobilized with uricase through a precipitation and crosslinking procedure. Such biosensor possesses a higher enzyme density, significantly larger contact area with reactants and could maintain the intact SACNT structure and its excellent conductivity after modification. The developed 3D SACNT array electrochemical biosensor benefits from high specific surface area, high electro-catalytic activity and large contact area with analytes, and demonstrates high sensitivity of 518.8 μA/(mM·cm^2), wide linear range of 100–1000 μM and low limit of detection of 1 μM for uric acid. Dynamic uric acid monitoring has been achieved using the presented biosensor. And the obtained results in serum samples had no significant difference compared with those obtained using the FDA-approved electrochemical analyzer (Paired T-test, $p > 0.05$). These demonstrated that the technology can potentially be applied in POC monitoring of other biomolecules to improve prognosis, diagnosis and treatment outcomes of metabolic diseases.

1. Introduction

Gout is a common and complex form of arthritis that affects a large population, which causes sudden, severe attacks of pain, swelling, redness and tenderness in the joints (Perez-Ruiz et al., 2015; Ragab et al., 2017). According to literature, the prevalence of gout is 1–4% of the general population worldwide, and in some countries and regions the prevalence may increase up to 10% (Kuo et al., 2015). The biological cause of gout is chronic elevation of serum uric acid levels above the saturation point for monosodium urate crystal formation (Lakshmi et al., 2011). Uric acid is an end product of purine metabolism in the human body and is in the range of 200–430 μM in healthy human serum, while in gout patients it could reach up to 430–570 μM (Ghosh et al., 2015; Schlesinger et al., 2009). Lasting high uric acid level may not only cause gout, but also lead to other severe diseases such as kidney diseases, cardiovascular diseases, and neurological diseases (Abou-Elela, 2017; Ghosh et al., 2015; Lakshmi et al., 2011). Therefore, it is necessary to examine uric acid levels for prognosis, diagnosis and treatment of a variety of diseases especially gout.

The first reported method for uric acid analysis was developed by Offer in 1894, who applied chemical oxidation of uric acid to reduce phosphotungstic acid to a tungsten blue chromophoric compound. This method suffered from poor specificity where cross-reaction from other compounds was common. To overcome this problem, researchers attempted to apply uricase to realize specific detection of uric acid. Based on the absorbance of quinone imine products from Trinder's reaction the uric acid level could be determined (Erden and Kilic, 2013). Gradually this enzymatic colorimetric method became gold standard of clinical uric acid testing and was widely accepted due to its high specificity. However, the complex procedures and cumbersome

* Corresponding author.
** Corresponding author. Precision Medicine and Healthcare Research Center, Tsinghua-Berkeley Shenzhen Institute(TBSI), Tsinghua University, Shenzhen, 518055, China.
E-mail addresses: hanwang@tsinghua.edu.cn (H. Wang), jcheng@tsinghua.edu.cn (J. Cheng).

https://doi.org/10.1016/j.bios.2021.113082
Received 12 January 2021; Received in revised form 3 February 2021; Accepted 4 February 2021
Available online 7 February 2021

instrumentation have hindered its application. Later on, many alternative techniques for uric acid sensing have been reported, aiming to improve the sensitivity, linear range, limit of detection or to realize rapid, high-throughput detection, such as chemiluminescence (Yu et al., 2011), high-performance liquid chromatography (HPLC) (Li et al., 2015; Zhao, 2015), enzymatic fluorescence (Azmi et al., 2015), capillary electrophoresis (Zhao et al., 2016a), weak measurement system (Zhang et al., 2018), surface plasma resonance (Zhang et al., 2016) and so on. Those techniques have been reported for testing uric acid in the laboratory with high sensitivity, however most of these techniques were restricted by complex sample pre-treatment, cumbersome instruments and long processing time (Erden and Kilic, 2013). Uric acid is mostly examined in the hospital laboratory after symptoms have already appeared, leading to possible delayed treatment. Moreover in metabolically disordered patients, uric acid level fluctuates dramatically (Schlesinger et al., 2009). Nowadays, with the emerging need of precision health, frequent detection and dynamic monitoring of uric acid is very important for gout prognosis, diagnosis and treatment (Abou-Elela, 2017; Vaidya et al., 2018).

POC testing, known for testing of blood chemistry, gases, electrolytes, and clotting, at or near the site of patient care, has advantages in short processing time, ease of use, portability, small sample consumption and capability to achieve real-time dynamic monitoring (Sista et al., 2008; Syedmoradi et al., 2017). It is a paradigm shift of diagnostic test from conventional central laboratory setting to near-patient setting. Therefore, POC testing provides actionable diagnostic information at the time needed, enabling informed decisions regarding diagnosis and treatment. Photometric POC testing methods have been extensively studied due to its convenient signal readout, however, most of these methods are much vulnerable to environmental variations such as skin thickness and not feasible for further miniaturization (Estevez et al., 2012). Electrochemical detection methods have been widely applied in POC applications for its high sensitivity, compact structure, and ease of integration. In electrochemistry method the redox reactions involving biomolecules cause electron transfer in the electrodes to generate reaction currents, and the electrical signals are analyzed to calculate biomolecule information (Hamann et al., 2007). Uric acid as one of the human metabolites has high electrocatalytic activity and is suitable for electrochemical detection. Therefore, electrochemistry method could provide a promising tool for real-time, convenient, rapid, and highly sensitive POC uric acid monitoring (Hadi and Rouhollahi, 2012; Kimmel et al., 2012).

There are two types of electrochemistry method, non-enzymatic and enzymatic electrochemistry. Non-enzymatic electrochemistry method utilizes different kinds of electro-active materials to improve the sensitivity of biomolecule detection, such as zero-dimensional materials carbon nanoparticles (Dutta et al., 2014) and SnO_2 quantum dots (Huang et al., 2013), one-dimensional material carbon nanotubes (Barsan et al., 2015), two-dimensional materials (Jiang and Du, 2014) and composites such as graphene/size-selected Pt nanocomposites (Sun et al., 2011), MoS_2/reduced graphene oxide (Xing and Ma, 2016a) and so on. However this method suffers from low specificity, because in human blood ascorbic acid (AA), dopamine (DA), and uric acid (UA) coexist and their oxidation peak currents are overlapped. Enzymatic electrochemistry method uses specific catalytic action of enzymes to obtain the biomolecule information in samples. Recently enzymatic electrochemistry method has attracted great attention for advantages such as high specificity, and could serve as a promising tool for specific detection of biomolecules. Nevertheless, current enzymatic electrochemistry methods have disadvantages of low sensitivity, narrow linear range, or high limit of detection (Erden and Kilic, 2013; Piermarini et al., 2013). Therefore, developing an enzymatic electrochemical biosensor with high sensitivity, wide linear range, low limit of detection and simple fabrication process for POC uric acid monitoring is in urgent need.

To achieve this goal, researchers have explored various types of electro-catalytic materials and enzyme immobilization methods for the working electrode, which plays the most critical role in enzymatic electrochemical sensing (Erden and Kilic, 2013). In recent years, carbon nanotubes (CNTs) have been widely applied in biomolecule detection due to their unique physical, electrical and chemical properties (Ahmad et al., 2015; Bandodkar et al., 2016; Han et al., 2014; Zhao et al., 2016b). CNTs have high aspect ratio, high mechanical strength, excellent chemical and thermal stability, and superior electronic and optical properties, which make CNTs important material in biosensors (Dang and Zhao, 2020; Yang et al., 2010). However, in electrochemical biosensors CNTs are typically used as thin layers that have limited contact area and enzyme immobilization space, which significantly affects their performance.

In this work, we report for the first time, design and fabrication of a novel enzymatic electrochemical biosensor based on 3D Super-Aligned Carbon NanoTube (SACNT) array. We report the successful development of an electrochemical biosensor with a 3D SACNT array working electrode by precipitation and crosslinking uricase on the 3D SACNT array for real-time uric acid monitoring. The novel biosensor preserves the intact SACNT structure and would provide high specific surface area, high electro-catalytic activity and large contact area with samples. To study the characteristics of the biosensor, we analyzed the surface structures of the working electrode and performed electrochemical tests of the biosensor with uric acid samples. We envision the presented method provides a promising tool for clinical prognosis, diagnosis and treatment of other metabolite disorders such as glucose, lactic acid, etc. in the future.

2. Materials and methods

2.1. Materials preparation

Chitosan (50,000–190,000 Da), uric acid (≥99%), surfactant (PEG-PPG-PEG), and glutaraldehyde (GA) solution (50% in H2O) were purchased from Sigma (Steinheim, Germany). Uricase (≥10 units/mg) was purchased from Macklin (Shanghai, China). Silver nanoparticles (AgNP) and amino functionalized carbon nanotubes (≥99%) were purchased from Yuanye Biology Company (Shanghai, China). Phosphate buffer solution (pH = 7.2–7.4) was from Solarbio (Beijing, China). All other chemicals used were of analytical grade. Double distilled water was used throughout the experiments. All electrochemical measurements were performed on the CHI660E electrochemical workstation (Chenhua, Shanghai, China).

2.2. Electrochemical detection mechanism

The developed electrochemical biosensor is based on the three-electrode system, which consists of a working electrode, a reference electrode and a counter electrode. As the following chemical equation (1) shows, the uric acid in the solvent is catalyzed by uricase on the working electrode and oxidized into allantoin, producing carbon dioxide and hydrogen peroxide (Numnuam et al., 2014).

$$\mathbf{uricacid} + \mathbf{H_2O} \overset{uricase}{\rightarrow} \mathbf{allantoin} + \mathbf{H_2O_2} + \mathbf{CO_2} \quad (1)$$

Then the produced H_2O_2 decomposes on the surface of the electrodes as equation (2) shows and the corresponding current is detected.

$$\mathbf{H_2O_2} \rightarrow \mathbf{O_2} + \mathbf{H^+} + 2e^- \quad (2)$$

2.3. System design

Fig. 1 shows the configuration of the developed 3D SACNT array electrochemical biosensor. This biosensor is comprised of two parts, the three-electrode system for uric acid sensing and the microfluidic module for introducing analytes (Fig. 1(A)). The working electrode in Fig. 1(B) is a 3D SACNT array sensing element, which is comprised of uricase,

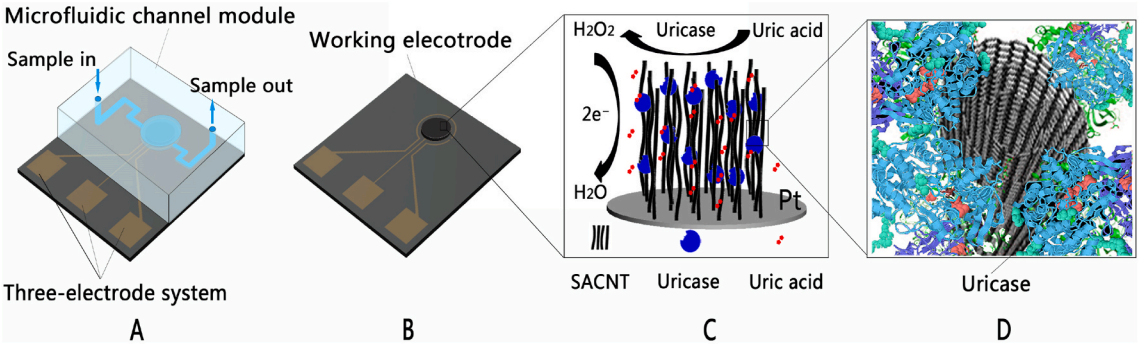

Fig. 1. Schematic illustration of the design and construction of the 3D SACNT array electrochemical biosensor for uric acid detection. (A) The electrochemical biosensor is composed of a three-electrode system, and a microfluidic channel module for introducing samples; (B) The three-electrode system fabricated on a silicon wafer and the SACNT array fixed on the working electrode; (C) Configuration of the 3D SACNT array sensing element in the working electrode; (D) Schematic illustration of uricase immobilized on SACNT.

SACNT, chitosan and glutaraldehyde as shown in Fig. 1(C-D). SACNTs are bundles of carbon nanotubes oriented perpendicular to a substrate. SACNT array's orderly 3D structure could not only increase enzyme immobilization density but also provide significantly larger contact area with reactants than regular CNTs. A photographic image of the biosensor is shown on Fig. S1. Besides, we were able to immobilize uricase directly on SACNTs through a precipitation and crosslinking procedure, other than modifying chemical functional groups that would damage SACNTs. Thus SACNTs could maintain the intact structure and excellent conductivity after modification (Chauhan and Pundir, 2011). Such SACNT array sensing element possesses three major advantages. First, SACNT array has high specific surface area and greatly increases contact area between analytes and immobilized enzymes. Second, SACNT array benefits from high electron conductivity and could significantly improve electro-catalytic activity by increasing electron transfer. Third, the stereoscopic 3D structure of the SACNT array could significantly enhance the density and stability of immobilized uricase and improve the sensitivity of uric acid detection. Therefore, the developed 3D SACNT array electrochemical biosensor could achieve high sensitivity and high stability detection of uric acid.

2.4. Fabrication of the SACNT array

The carbon nanotube was grown with the chemical vapor deposition method. An iron catalyst was evaporated onto a silicon substrate by electro-beam evaporation. The substrate was placed into a quartz tube furnace at 700 °C, and acetylene was introduced. The growth happened under a low-pressure state for 10 min. After about 10 min growth, an SACNT array of 300 μm could be obtained.

2.5. Fabrication of the three-electrode biosensor

The biosensor was prepared by microfabrication as shown in Fig. 2. First, the silicon wafer was rinsed with acetone and isopropyl alcohol followed by plasma enhanced chemical vapor deposition (PECVD) to form a dense oxide film on the surface of silicon wafer. Then a positive photoresist (Shipley S1818, Rohm and Haas Electronic Materials Co., Marlborough, MA) was spin-coated at 4000 rpm for 30 s. The positive photoresist was soft-baked at 110 °C for 5 min. UV exposure system (MA-10, Mikasa CO., LTD., Tokyo, Japan) was applied to pattern the photoresist, which was then developed in MF-319, and hard-baked for 5 min at 130 °C. After that, a 30 nm thick Cr and 50 nm thick Pt was sputtered (CFS-4ES-231, Shibaura Engineering Works CO., LTD., Tokyo, Japan) onto the wafer surface. The electrodes were formed using a lift-off process. Finally, the SACNT array that was grown on silicon wafer separately was cut out to the size of the working electrode by laser and transferred to the working electrode using conductive silver paste. Last,

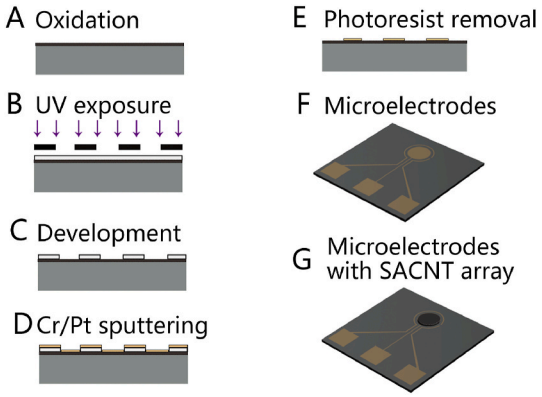

Fig. 2. Fabrication procedures of the SACNT array biosensor.

the microfluidic module which was made by polydimethyl siloxane (PDMS) was cast molded separately using master mold from a 3D ultraviolet curing printer.

2.6. Modification of the working electrode and optimization of experimental conditions

The working electrode was fabricated by the aforementioned micro fabrication procedures, followed by surface modification to immobilize uricase on SACNT through a precipitation and crosslinking process. First, chitosan/CNTs solution was prepared by adding 5 mg amino functionalized carbon nanotubes into a 2 ml chitosan solution (0.2% wt) with ultrasonic mixing for 10 min to achieve complete dispersion. Then 1 mg uricase was added to Chitosan/CNTs solution (50 μl) to obtain Uricase/Chitosan CNTs solution. A drop of Uricase/Chitosan CNTs solution (3 μl) was introduced onto the SACNT array working electrode, dried at room temperature, and then 3 μl glutaraldehyde solution (5%) was added onto the working electrode. The above mixture was incubated at room temperature to crosslink for 1 h, and the GA/Uricase/Chitosan/SACNT/Pt electrode was thus prepared. The working electrode was gently rinsed 3 times with PBS by pipetting and then the modified biosensor was stored in refrigerator at 4 °C until use. GA/Chitosan/SACNT/Pt electrode was also prepared through the same procedures without adding uricase onto the working electrode. Conventional immobilization methods utilize covalent bonding to achieve enzyme immobilization. As a result, strong oxidants such as nitric acid and sulfuric acid are usually applied to CNTs to produce functional groups, which inevitably damages CNTs structures (Alwarappan et al., 2010; Gao et al., 2012). Our immobilization method utilizes a precipitation and crosslinking procedure without using any strong oxidants.

Therefore, intact SACNT structure is preserved and excellent SACNT electron conductivity is maintained. For optimization of the experimental conditions, the concentration of uricase solution was one of the most important aspects. Different concentrations of uricase solution varying from 10 to 30 mg/ml with a 5 mg/ml interval were applied to modify the working electrodes. Those electrodes were evaluated by introducing 100 μl uric acid solution (300 μM) onto the working electrodes and the oxidation peak currents of the uric acid solution were investigated.

2.7. Scanning electron microscopy and confocal microscopy of the modified SACNT array biosensor

Scanning electron microscopy (SEM) studies of bare SACNT/Pt electrode and enzyme modified SACNT array electrode were carried out to confirm immobilization of uricase. The electrodes were cut into small pieces with a dicing saw and placed on a copper disc. Gold particles were deposited on the surface using a spray machine and electron micrographs were recorded. Confocal microscopy study of GA/Uricase/Chitosan/SACNT/Pt electrode was carried out to confirm the spatial distribution of immobilized uricase, and the 3D profile of the GA/Uricase/Chitosan/SACNT/Pt electrode was reconstructed.

2.8. Electrochemical characterization of the modified SACNT array biosensor

Cyclic voltammetry studies were conducted with the SACNT array biosensor using a CHI660E electrochemical workstation. The three-electrode system of the biosensor utilized GA/Uricase/Chitosan/SACNT/Pt as the working electrode, Ag/AgCl as the reference electrode and Pt as the counter electrode. Firstly, control experiments between GA/Uricase/Chitosan/SACNT/Pt electrode, GA/Chitosan/SACNT/Pt electrode and bare electrode were studied by introducing 100 μl uric acid solution (300 μM) into the working electrodes and recording the cyclic voltammetry response, respectively. Secondly, to further study the characteristics of the modified SACNT array biosensor, cyclic voltammograms were recorded by introducing 100 μl phosphate buffer solution (0.01 M, pH = 7.4) into the working electrode at scanning rates ranging from 10 to 200 mV/s with a 20 mV interval. The potential range during cyclic voltammetry tests was between −0.40 and 0.40 V. Thirdly, to evaluate the performance of the 3D SACNT array biosensor in uric acid detection, cyclic voltammograms were recorded after introducing 100 μl uric acid solutions (concentration varying from 1 μM to 2000 μM) into the working electrode at room temperature (25 °C). After each measurement, the working electrode was cleaned three times with DI water. The potential range during cyclic voltammetry tests for uric acid detection was set between −0.40 and 0.60 V and the scanning rate was set to 50 mV/s. All cyclic voltammetry data was processed using MATLAB 2014 (MathWorks, Natick, MA) and Origin 8.0 (OriginLab Corporation, Northampton, MA).

2.9. Specificity studies and dynamic uric acid monitoring of the modified SACNT array biosensor

Firstly, to study the specificity of the modified SACNT array biosensor, amperometric I–t measurement of the biosensor was carried out by adding three different interferents such as glucose at 5 mM, lactic acid at 0.5 mM and ascorbic acid at 0.1 mM, respectively, into 100 μl uric acid solution at 100 μM. The concentration of each interferent was chosen based on the average concentration level in health human blood. Secondly, to evaluate the dynamic uric acid monitoring performance of the biosensor, amperometric I–t curve for measuring uric acid at different concentrations in PBS solution (pH = 7.4, 0–700 μM) was tested. Series of uric acid samples with different concentrations were prepared and withdrew into the working electrode one after another by a syringe pump (LSP02-1B, Longer Precision Pump Co., Ltd, Hebei, China). The applied potential was 0.12 V. The flow rate was 500 μl/min.

2.10. Stability studies of the modified SACNT array biosensor

To evaluate the stability of the GA/Uricase/Chitosan/SACNT/Pt working electrode, after uric acid testing as described in the previous session, the biosensor was washed by PBS buffer, dried and stored in a refrigerator at 4 °C for 4 weeks. Then the biosensor was retrieved and the performance was investigated by cyclic voltammetry. The same procedures were performed to repeat uric acid detection experiments using varying concentrations of uric acid samples from 1 μM to 2000 μM. The potential range during cyclic voltammetry tests was set to the same range between −0.40 and 0.60 V and the scanning rate was also set to 50 mV/s. The measured oxidation currents and sensitivity of the GA/Uricase/Chitosan/SACNT/Pt working electrode before and after storage were compared.

2.11. Analysis of real samples

To investigate the feasibility of the developed 3D-structured SACNT array biosensor for uric acid detection in biological fluids, serum samples from healthy human volunteers spiked with uric acid to final concentrations of 300, 400, 500, 600 μM were measured by our biosensor, and compared with the FDA-approved electrochemical analyzer (Benecheck, Taiwan, China). The serological samples were collected in anticoagulant tubes and used immediately after collection.

3. Results and discussion

The SACNT array electrochemical biosensor was successfully fabricated and modified with enzymes. After 10 min growth, an SACNT array with the height of CNT achieving 300 μm was obtained. According to our statistics about the SACNT by transmission electron microscopy, the diameter of the carbon nanotube was 7–11 nm and the wall number was between 6 and 10.

Fig. 3(A-D) and Fig. S2 show the side and surface profile of the SACNT/Pt working electrode before and after uricase immobilization. Before enzyme immobilization the inside of SACNT array was vertically aligned while the surface of SACNT array was staggered, as seen from the SEM image in Fig. 3(A-B). After enzyme immobilization, the inside and surface of the SACNT array were covered by clusters or ellipsoidal particles, as can be seen from Fig. 3(C-D) and Fig. S2(C-D). The immobilization of uricase on the GA/Uricase/Chitosan/SACNT/Pt electrode was confirmed from SEM images of the surface of working electrode before and after uricase immobilization. The reconstructed 3D image of GA/Uricase/Chitosan/SACNT/Pt electrode from confocal microscopy indicates that uricase was evenly immobilized on the upper surface and sides of the working electrode (Fig. S3). As mentioned before, conventional immobilization methods utilize strong oxidants to produce functional groups on CNTs for covalent bonding with enzymes at the cost of damaging the CNTs structure. Our method immobilizes uricase to the SACNT array by precipitation and crosslinking using glutaraldehyde, which causes no damage to the SACNT array. This method could also be applied in immobilization of other electro-catalytic materials in enzymatic biosensors as compared to covalent bonding methods. The cyclic voltammetry response of biosensors modified by different methods were evaluated in 300 μM uric acid solution at the scanning rate of 50 mV/s. As seen in Fig. 3(E), the GA/Uricase/Chitosan/SACNT/Pt electrode exhibited excellent response for detection of uric acid and a pair of redox peaks was observed with oxidation at 0.12 V and reduction at −0.20 V. For the GA/Chitosan/SACNT/Pt electrode, no obvious redox peaks were observed due to absence of uricase on the working electrode. The current response of bare electrode was even weaker compared to the other two modified electrodes. These results demonstrated outstanding electrocatalytic performance of the GA/Uricase/Chitosan/SACNT/Pt electrode for uric acid detection. For optimization of the concentration of

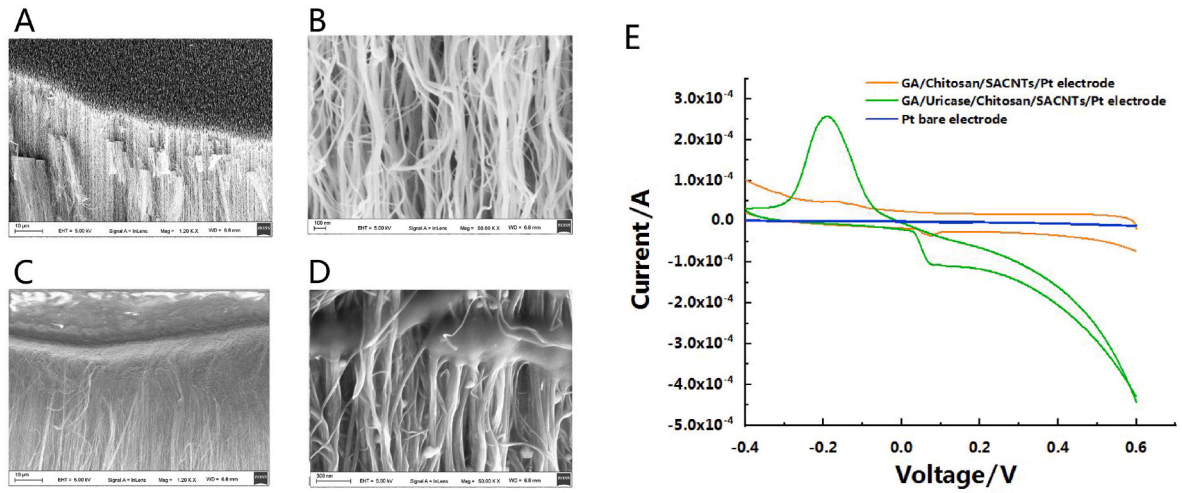

Fig. 3. SEM images of the SACNT side at (A) 12,000 times magnification and (B) 100,000 times magnification of SACNT/Pt working electrode before uricase immobilization; SEM images the SACNT side at (C) 12,000 times magnification and (D) 100,000 times magnification of GA/Uricase/Chitosan/SACNT/Pt electrode after uricase modification. Cyclic voltammetry response of GA/Chitosan/SACNT/Pt electrode, GA/Uricase/Chitosan/SACNT/Pt electrode and Pt bare electrode in PBS (pH = 7.4) containing 300 μM uric acid solution at the scanning rate of 50 mV/s (E).

uricase solution, the peak response currents of uric acid increased gradually as the concentration of uricase solution increased and then remained steady beyond 20 mg/ml (Fig. S4). Therefore, the concentration of uricase solution of 20 mg/ml was adopted as the optimal concentration for the following experiments.

Fig. 4(A-B) shows the cyclic voltammograms of the biosensor under different scanning rates. The oxidation current increased as the scanning rate increased from 10 to 200 mV/s with 20 mV/s interval (Fig. 4(A)). The peak oxidation current of all cyclic voltammetry curves increased in a linear manner as the scanning rate increased (Fig. 4(B)). This suggests that electron transfer at the GA/Uricase/Chitosan/SACNT/Pt electrode was surface adsorption controlled, which means the rate of the redox reaction depends on the adsorption rate between the reactants and the active substances on the surface of the working electrode. The current

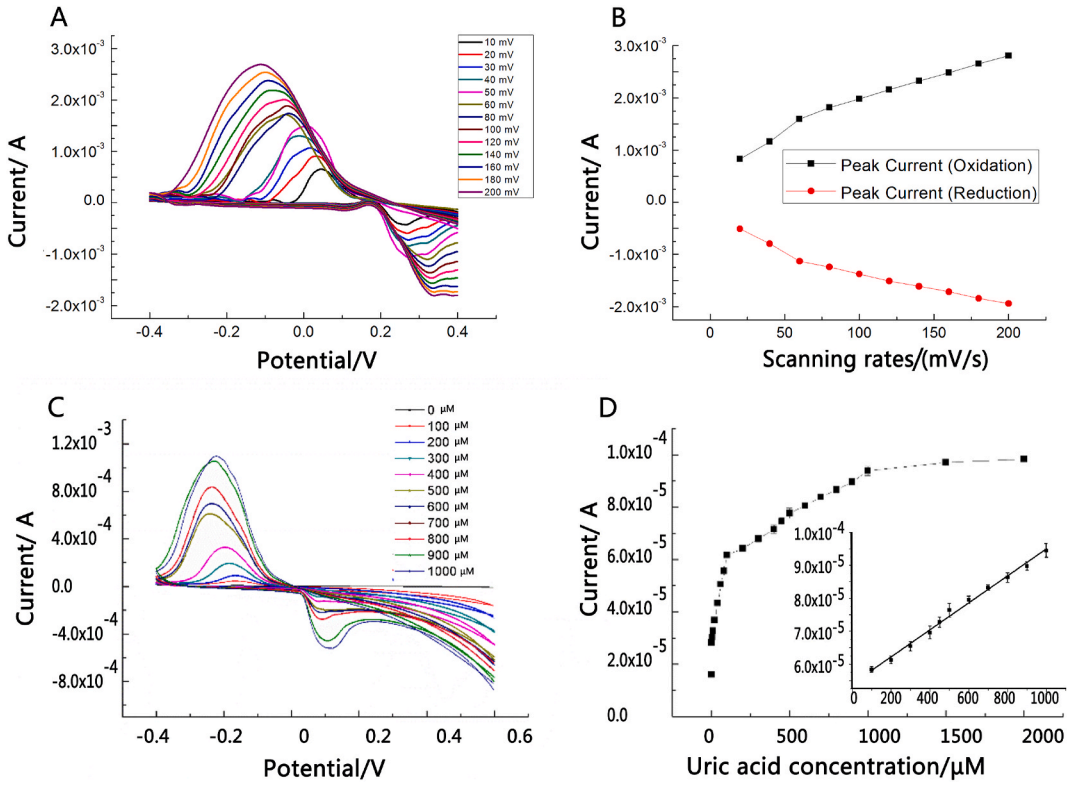

Fig. 4. Cyclic voltammetry results of the biosensor under different scanning rates and in uric acid solutions of different concentrations. (A) Effect of the scanning rate on the redox reaction behavior for the GA/Uricase/Chitosan/SACNT/Pt electrode. Scanning rates: 10, 30, 50, 80, 100, 120, 140, 160, 180 mV/s. The oxidation current increased as the scanning rate increased. (B) Plot of peak oxidation and reduction currents versus scanning rates. The peak oxidation current increased as the scanning rate increased in a linear manner. (C) Cyclic voltammetry curve of GA/Uricase/Chitosan/SACNT/Pt electrode in 0.01 M PBS (pH = 7.4) containing uric acid with concentrations from 0 to 1000 µM. (D) Peak oxidation currents plotted as functions of uric acid concentration. Insert is linear curve fitting between currents and uric acid concentration, coefficient of association $R^2 = 0.9956$. ($N = 4$) (Diameter of working electrode = 3 mm, sensitivity = 518.8 µA/(mM·cm^2)).

response of the GA/Uricase/Chitosan/SACNT/Pt electrode to different concentrations of uric acid was investigated using phosphate buffer (pH = 7.4).

The cyclic voltammograms of different concentrations of uric acid solutions are presented in Fig. 4(C-D). The response time was around 9 s at the scanning rate of 50 mV/s, which was close to the literature (see Table 1). Fig. 4(D) shows the peak oxidation currents corresponding to different concentrations of uric acid solutions varying from 1 μM to 2000 μM. As seen from Fig. 4(D), the peak oxidation current increased sharply at low concentrations and linearly from 100 μM to 1000 μM, and finally reached saturation when the uric acid concentration was more than 1000 μM. The insert in Fig. 4(D) shows curve fitting between peak oxidation currents and uric acid concentrations. The current response of the 3D SACNT array uric acid biosensor was linear in the range from 100 μM to 1000 μM with a correlation coefficient of 0.9956. The limit of detection of the biosensor was 1 μM and the sensitivity was 518.8 μA/(mM·cm^2), of which the linear range and sensitivity of the biosensor was superior than most of the previously reported enzymatic electrochemistry biosensors (see Table 1). The standard deviation of the measured peak oxidation currents is 4.2×10^{-7} A as shown in Fig. 4(D) insert, demonstrating excellent repeatability of the 3D SACNT array biosensor. From Table 1, we further confirm that nonenzymatic electrochemistry methods could achieve lower limit of detection than enzymatic electrochemistry methods. While enzymatic electrochemistry methods typically have wider linear range. The structure and material of working electrode play important roles in the performance of enzymatic electrochemical methods as shown in the table. Two-dimensional working electrodes like glassy carbon electrodes have a large sensing area, however lacks sufficient limit of detection and linear ranges (Arora et al., 2011; Ghosh et al., 2015). Three-dimensional structure electrodes such as Nafion/Uricase/ZnO/Ag/Si working electrode exhibited similar performance except lower sensitivity compared to our method, possibly due to its 3D nanosheet ZnO structure and the catalytic activity of Ag nanoparticles (Ahmad et al., 2015). Our work is a step forward in building three-dimensional working electrodes as the SACNTs have larger contact area between uricase and uric acid, which is helpful in improving its sensitivity. This suggests that 3D structure and catalytic nanoparticles of the working electrode could enhance the performance of electrochemical biosensors. However, most of these techniques suffer from either high limit of detection or narrow linear range (Arora et al., 2011; Ghosh et al., 2015). This work demonstrated a 3D SACNT array uric biosensor with low limit of detection and wide linear range which could meet the clinical requirement for gout diagnosis.

To evaluate the specificity of the fabricated uric acid biosensor, amperometric response was measured at the applied potential of 0.12 V by introducing uric acid and other interferents. Fig. 5(A) showed that these interfering species exhibited no effect on the biosensor response, indicating that our fabricated biosensor was feasible for specific detection of uric acid in the presence of other interferents. Fig. 5(B) shows the amperometric I–t curve for dynamic measurement of uric acid with the biosensor. The uric acid samples at different concentration gradients ranging from 0 to 600 μM in PBS solution (pH = 7.4) were tested. It can be seen that the amplitude of oxidation current increases as the uric acid concentration goes up. Upon the change of uric acid solution concentration by replenishing with new medium on the working electrode through micro-channels, the amperometric change of the biosensor was within 300 s. This result demonstrates the sensitive and quick measurement capability of the GA/Uricase/Chitosan/SACNT/Pt biosensor that facilitates dynamic uric acid monitoring. As seen in Fig. 5(C), after 4 weeks of storage in a 4 °C refrigerator, the performance of the 3D SACNT array electrochemical biosensor remained largely unchanged. After storage, the absolute values of peak oxidation currents at the same concentration of uric acids were lower by 3.02% compared to those before storage. The slope of the peak oxidation curve after storage, which directly correlates to the sensitivity of the biosensor, was very close to that before storage, which were 495.3 and 518.8 μA/(mM·cm^2), respectively. This indicates that even after 4 weeks storage, the GA/Uricase/Chitosan/SACNT/Pt electrode maintained nearly the same sensitivity with only 3.02% decrease in absolute peak oxidation current values. These results demonstrate that the modified biosensor of GA/Uricase/Chitosan/SACNT/Pt possesses excellent stability for analytical applications. To further confirm the feasibility of the developed 3D-structured SACNTs array biosensor for uric acid detection in biological fluids, serum samples from healthy human volunteers spiked with uric acid were tested. The results were also compared with those obtained using the FDA-approved electrochemical analyzer, and no significant difference was found using Paired T-test (Fig. 5(D), $p > 0.05$). The results demonstrated that the accuracy of the 3D-structured SACNT array biosensor is sufficient for uric acid detection in real samples.

From the above results, the 3D SACNT array biosensor of GA/Uricase/Chitosan/SACNT/Pt demonstrated high sensitivity, wide linear range and low limit of detection, which could meet the needs of gout diagnosis in clinics or even at home. The biosensor employed high catalytic activity and high electron conductivity of the SACNT array. As reported, nanomaterials such as CNTs, gold nanoparticles, graphene and so on have high catalytic activity and their high conductive properties also promote electron transfer efficiency during the electrochemical redox reaction (Xing and Ma, 2016b), which improves the sensitivity of the developed biosensor. Moreover, the 3D SACNT structure of the working electrodes also contributes to the biosensor's superior performance of biomolecule detection. Conventional enzymatic electrochemical biosensors typically apply a thin layer of composites as the working electrode, such as glassy carbon electrodes or other paper-based printed electrodes. These electrodes are limited by the number of fixed enzymes and the contact area between target reactants and fixed enzymes per unit area, and also suffer from large sensor size. Ahmad et al. reported a 3D structure-like ZnO nanosheet biosensor and the biosensor also showed good results but lower sensitivity than ours (Ahmad et al., 2015). Therefore, nanomaterials with high catalytic activity and three-dimensional structure of the working electrode could help to promote the biosensors' performance in sensitivity, linear range and limit of detection, etc.

Table 1
Comparison of the analytical performance of the GA/Uricase/Chitosan/SACNT/Pt electrode in this work with those of other electrochemical electrodes reported in the literature.

Electrode materials	Enzyme uricase	Sensitivity	Linear range/μM	Response time/s	LOD/μM	References
Au/Pd/RGO	No	None	0.1–350	None	0.02	Jiang and Du (2014)
graphene/Pt nanocomposite	No	411.9 μA/mM	0.05–11.85	0.6	0.05	Sun et al. (2011)
Nafion/Uricase/ZnO/Ag/Si	Yes	129.81 μA/(mM·cm^2)	50–2000	5	0.019	Ahmad et al. (2015)
Prussian-blue graphite ink	Yes	2.32 μA/mM	0–1000	None	None	Kim et al. (2015)
Uricase/tetrapod-shaped ZnO	Yes	80.0 μA/(mM·cm^2)	0.8–3490	9	0.8	Lei et al. (2012)
printed electrode/Prussian blue	Yes	None	30–300	None	10	Piermarini et al. (2013)
NiO/Pt/Ti/glass	Yes	1278.48 μA/mM	50–1000	5	170	Arora et al. (2011)
Nafion/uricase/ferrocene/GCE	Yes	1780 μA/mM	0.5–60	5	0.23	Ghosh et al. (2015)
GA/Uricase/Chitosan/SACNT/Pt	Yes	518.8 μA/(mM·cm^2)	100–1000	9	1.0	This work

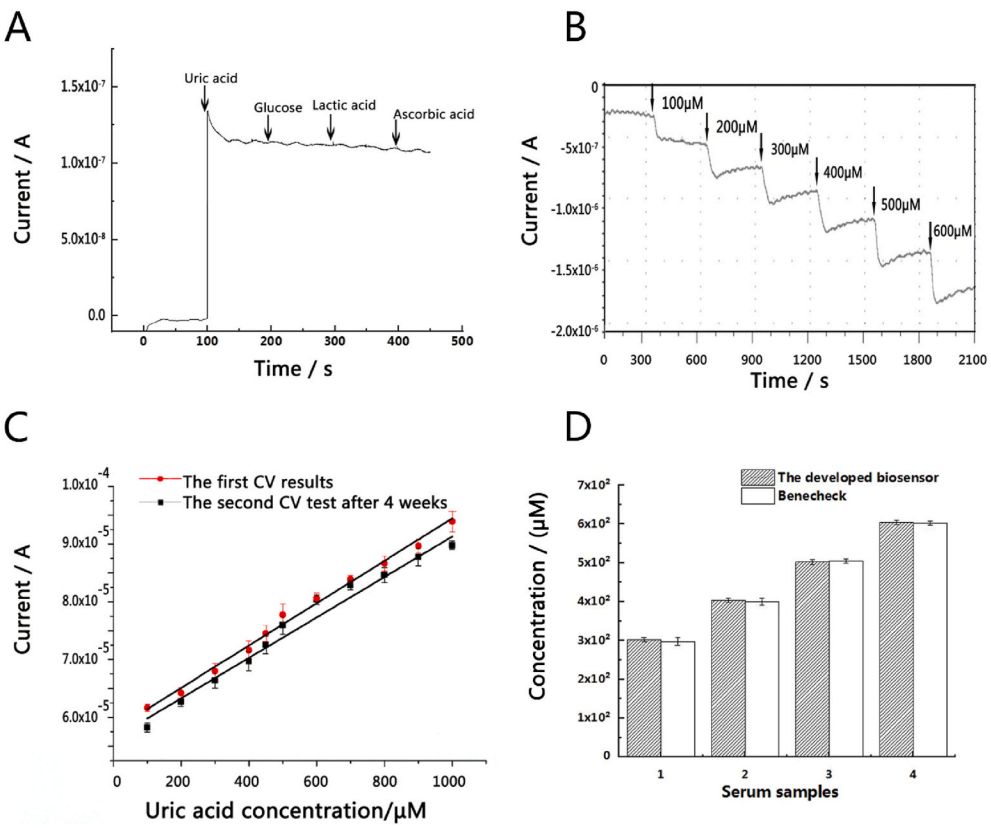

Fig. 5. (A) Interference tests of the uric acid biosensor upon addition of uric acid (300 μM), glucose (5 mM), lactic acid (0.5 mM), ascorbic acid (0.1 mM) in100 μl PBS solution. (B) Amperometric I–t curve for dynamic monitoring of uric acid with the biosensor in 100 μl PBS solution (pH = 7.4), the applied potential was 0.12 V. Each addition of uric acid solutions was provided by the pump at 1 ml/min with a time interval of 300s and the uric acid concentration was increased from 100 to 600 μM. (C) Stability testing results of the biosensor in uric acid solution before (red dot, $N = 4$) and after (black square, $N = 3$) storage in a refrigerator at 4 °C for 4 weeks. (D) Determination of uric acid in real serum samples collected from human via our biosensor compared with the FDA-approved BeneCheck PLUS system ($N = 4$). The statistical result showed no significant difference (Paired T-test, $p > 0.05$). (For interpretation of the references to color in this figure legend, the reader is referred to the Web version of this article.)

4. Conclusion

In this work, we have successfully developed a 3D SACNT array electrochemical biosensor for POC uric acid testing with high sensitivity and high stability. The GA/Uricase/Chitosan/SACNT/Pt electrode exhibits high sensitivity of 518.8 μA/(mM·cm^2), wide linear range of 100 μM–1000 μM, and low limit of detection of 1 μM. Compared to other reports, the major innovation of the reported electrochemical biosensor is to utilize 3D SACNT array with enzymes immobilized by a precipitation and crosslinking procedure, which delivers superior performance of high sensitivity, wide detection range, low limit of detection and short response time. Moreover, we have successfully realized dynamic monitoring of uric acid in continuous flow with the biosensor, which would be of great help in early diagnosis and prevention of gout. The biosensor is also ready for mass production for its easy fabrication based on standard micro fabrication procedures. Besides researches could continue to explore various types of 3D structure materials with suitable porous sites for enzymes to be immobilized inside and outside the 3D structure, such as nickel foam and graphite sheets. Additionally, this detection system could be expanded to detect other biomolecules such as different types of metabolites in diagnosis of metabolic disorders. Finally, the system could integrate other modules to realize POC real-time monitoring of various biomolecules.

In conclusion, we have successfully developed a 3D SACNT array electrochemical biosensor for POC uric acid monitoring, which could meet the emerging clinical need of frequent and convenient uric acid detection, and help to improve diagnosis and treatment outcomes of metabolic diseases such as gout. And our results demonstrated that the accuracy and reliability of the 3D-structured SACNTs array biosensor is sufficient for the determination of uric acid in real sample. And this biosensor holds great promise for potential applications in monitoring the dynamic trend of various biomolecules such as glucose, lactic acid and so on in the future.

Declaration of competing interest

The authors declare that they have no known competing financial interests or personal relationships that could have appeared to influence the work reported in this paper.

Acknowledgment

This project was supported by the National Natural Science Foundation of China grant 81801791, National Key R&D Program of China grant 2020YFB2009000, Shenzhen Municipal Development and Reform Commission, Shenzhen Engineering Laboratory for Precision Medicine and Healthcare, Grant Number: SDRC [2015]1950 and Shenzhen Municipal Development and Reform Commission Subject construction project [2017]1434.

Appendix A. Supplementary data

Supplementary data to this article can be found online at https://doi.org/10.1016/j.bios.2021.113082.

CRediT author statement

Muqun Yang: Data curation, Writing- Original draft preparation, Visualization, Investigation, Software.

Han Wang: Conceptualization, Methodology, Supervision, Writing-Reviewing and Editing , Funding acquisition.

Peng Liu: Methodology, Resources , Writing- Reviewing.

Jing Cheng: Methodology, Supervision, Reviewing and Editing, Funding acquisition.

References

Abou-Elela, A., 2017. J. Adv. Res. 8 (5), 513–527.

Ahmad, R., Tripathy, N., Jang, N.K., Khang, G., Hahn, Y.-B., 2015. Sensor. Actuator. B Chem. 206, 146–151.
Alwarappan, S., Liu, G., Li, C.Z., 2010. Nanomed. Nanotechnol. 6 (1), 52–57.
Arora, K., Tomar, M., Gupta, V., 2011. Biosens. Bioelectron. 30 (1), 333–336.
Azmi, N.E., Ramli, N.I., Abdullah, J., Abdul Hamid, M.A., Sidek, H., Abd Rahman, S., Ariffin, N., Yusof, N.A., 2015. Biosens. Bioelectron. 67, 129–133.
Bandodkar, A.J., Jeerapan, I., You, J.-M., Nuñez-Flores, R., Wang, J., 2016. Nano Lett. 16 (1), 721–727.
Barsan, M.M., Ghica, M.E., Brett, C.M.A., 2015. Anal. Chim. Acta 881, 1–23.
Chauhan, N., Pundir, C.S., 2011. Anal. Biochem. 413 (2), 97–103.
Dang, X., Zhao, H., 2020. Talanta 210, 120678.
Dutta, D., Chandra, S., Swain, A.K., Bahadur, D., 2014. Anal. Chem. 86 (12), 5914–5921.
Erden, P.E., Kilic, E., 2013. Talanta 107, 312–323.
Estevez, M.C., Alvarez, M., Lechuga, L.M., 2012. Laser Photon. Rev. 6 (4), 1–25.
Gao, C., Guo, Z., Liu, J.-H., Huang, X.-J., 2012. Nanoscale 4 (6), 1948–1963.
Ghosh, T., Sarkar, P., Turner, A.P., 2015. Bioelectrochemistry 102, 1–9.
Hadi, M., Rouhollahi, A., 2012. Anal. Chim. Acta 721, 55–60.
Hamann, C.H., Hamnett, A., Vielstich, W., 2007. Weinheim: Wiley. (XVIII).
Han, H.S., You, J.M., Seol, H., Jeong, H., Jeon, S., 2014. Sensor. Actuator. B Chem. 194 (194), 460–469.
Huang, Q., Hu, S., Zhang, H., Chen, J., He, Y., Li, F., Weng, W., Ni, J., Bao, X., Lin, Y., 2013. Analyst 138 (18), 5417.
Jiang, J., Du, X., 2014. Nanoscale 6 (19), 11303–11309.
Kim, J., Imani, S., de Araujo, W.R., Warchall, J., Valdes-Ramirez, G., Paixao, T.R., Mercier, P.P., Wang, J., 2015. Biosens. Bioelectron. 74, 1061–1068.
Kimmel, D.W., LeBlanc, G., Meschievitz, M.E., Cliffel, D.E., 2012. Anal. Chem. 84 (2), 685–707.
Kuo, C.F., Grainge, M.J., Zhang, W., Doherty, M., 2015. Nat. Rev. Rheumatol. 11 (11), 649–662.
Lakshmi, D., Whitcombe, M.J., Davis, F., Sharma, P.S., Prasad, B.B., 2011. Electroanalysis 23 (2), 305–320.
Lei, Y., Liu, X., Yan, X., Song, Y., Kang, Z., Luo, N., Zhang, Y., 2012. J. Nanosci. Nanotechnol. 12 (1), 513–518.
Li, X.-L., Li, G., Jiang, Y.-Z., Kang, D., Jin, C.H., Shi, Q., Jin, T., Inoue, K., Todoroki, K., Toyo'oka, T., Min, J.Z., 2015. J. Chromatogr. B 1002, 394–398.
Numnuam, A., Thavarungkul, P., Kanatharana, P., 2014. Anal. Bioanal. Chem. 406 (15), 3763–3772.
Perez-Ruiz, F., Dalbeth, N., Bardin, T., 2015. Adv. Ther. 32 (1), 31–41.
Piermarini, S., Migliorelli, D., Volpe, G., Massoud, R., Pierantozzi, A., Cortese, C., Palleschi, G., 2013. Sensor. Actuator. B Chem. 179, 170–174.
Ragab, G., Elshahaly, M., Bardin, T., 2017. J. Adv. Res. 8 (5), 495–511.
Schlesinger, N., Norquist, J.M., Watson, D.J., 2009. J. Rheumatol. 36 (6), 1287–1289.
Sista, R., Hua, Z., Thwar, P., Sudarsan, A., Srinivasan, V., Eckhardt, A., Pollack, M., Pamula, V., 2008. Lab Chip 8 (12), 2091–2104.
Sun, C.L., Lee, H.H., Yang, J.M., Wu, C.C., 2011. Biosens. Bioelectron. 26 (8), 3450–3455.
Syedmoradi, L., Daneshpour, M., Alvandipour, M., Gomez, F.A., Hajghassem, H., Omidfar, K., 2017. Biosens. Bioelectron. 87, 373–387.
Vaidya, B., Bhochhibhoya, M., Nakarmi, S., 2018. Biomed. Rep. 9 (1), 60–64.
Xing, L., Ma, Z., 2016a. Microchim. Acta 183 (1), 257–263.
Xing, L., Ma, Z., 2016b. Prog. Chem. 28 (11), 1705–1711.
Yang, W., Ratinac, K.R., Ringer, S.P., Thordarson, P., Gooding, J.J., Braet, F., 2010. Angew Chem. Int. Ed. Engl. 49 (12), 2114–2138.
Yu, J., Wang, S., Ge, L., Ge, S., 2011. Biosens. Bioelectron. 26 (7), 3284–3289.
Zhang, P., Liu, L., He, Y., Chen, X., Ma, K., Wei, D., Wang, H., Shao, Q., 2018. Sensor. Actuator. B Chem. 272, 69–78.
Zhang, Y., Li, D., He, Y., Shen, Z., He, Q., 2016. Opt. Lett. 41 (22), 5409–5412.
Zhao, J., 2015. Biomed. Chromatogr. 29 (3), 410–415.
Zhao, M., Zhou, M.F., Feng, H., Cong, X.X., Wang, X.L., 2016a. Chromatographia 79 (13–14), 911–918.
Zhao, Z., Sun, Y., Li, P., Zhang, W., Lian, K., Hu, J., Chen, Y., 2016b. Talanta, S0039914016303988.